Atomic collapse in pseudospin-1 systems

Chen-Di Han,[1] Hong-Ya Xu,[1] Danhong Huang,[2] and Ying-Cheng Lai[1,3,*]
[1]*School of Electrical, Computer and Energy Engineering, Arizona State University, Tempe, Arizona 85287, USA*
[2]*Air Force Research Laboratory, Space Vehicles Directorate, Kirtland Air Force Base, New Mexico 87117, USA*
[3]*Department of Physics, Arizona State University, Tempe, Arizona 85287, USA*

(Received 11 February 2019; revised manuscript received 23 April 2019; published 17 June 2019)

We investigate atomic collapse in pseudospin-1 Dirac material systems whose energy band structure constitutes a pair of Dirac cones and a flat band through the conic intersecting point. We obtain analytic solutions of the Dirac-Weyl equation for the three-component spinor in the presence of a Coulomb impurity and derive a general criterion for the occurrence of atomic collapse in terms of the normalized strength of Coulomb interaction and the angular momentum quantum number. In particular, for the lowest angular momentum state, the solution coincides with that for pseudospin-1/2 systems, but with a reduction in the density of resonance peaks. For higher angular momentum states, the underlying pseudospin-1 wave functions exhibit a singularity at the point of zero kinetic energy. Divergence of the local density of states associated with the flat band leads to an inverse square type of singularity in the conductivity. These results provide insights into the physics of the two-body problem for relativistic quantum pseudospin-1 quasiparticle systems.

DOI: 10.1103/PhysRevB.99.245413

I. INTRODUCTION

Consider a relativistic quantum system in the presence of a Coulomb impurity, e.g., a nucleus. When the potential field is sufficiently strong, a particle and an antiparticle pair (e.g., an electron and a positron) will be created. The antiparticle becomes free, but the particle will collapse at the nucleus in the sense that the two will form a resonant, quasibound state of a finite lifetime. Semiclassically, the particle trajectory will spiral inward toward the nucleus [1–3], similar to the phenomenon of Landau fall in nonrelativistic quantum mechanics [4]. After the collapse, the particle trajectory will spiral out, couple to the antiparticle, and move away from the nucleus [5,6]. From the energy point of view, the originally discrete energy levels are turned into resonant states with finite lifetimes.

A necessary condition for atomic collapse to occur is that the relativistic quantum effects are strong enough to lead to a reconstruction of the Dirac vacuum. This can happen for a super-heavy nucleus [1,2]. Theoretically, the collapse phenomenon can be understood by examining the solution of the Dirac equation for a hydrogenlike atom with a Coulomb potential of the form $-Z/r$, where Z is the atomic number or the nuclear charge. An exact solution of the energy levels indicates that the energy becomes complex for $Z > 1/\alpha_0$, where $\alpha_0 \equiv e^2/(\hbar c) \approx 1/137$ is the fine structure constant. The physical picture for atomic collapse is that, as the nuclear charge Z increases, the eigenenergies of the discrete states enter the negative energy continuum one after another, transforming these states into resonances with complex eigenenergies, where the lifetime of a resonant state is proportional to the inverse of the imaginary part of the eigenenergy. Mathematically, the $1/r$ singularity associated with the Coulomb potential makes the Dirac operator non-Hermitian so that the Dirac equation breaks down in the vicinity of the singularity. One may use a regularized form of the potential to make the Dirac equation valid, but even after the singularity has been removed, the eigenenergies would still become complex for sufficiently large values of Z. Analyses carried out many decades ago [1,2] placed the following requirement for atomic collapse to occur: $Z > 170$, which is not possible for any known elements.

For any natural element, the fine structure constant α_0 is two orders of magnitude smaller than unity, making the required nuclear charge unrealistically large for generating atomic collapse. The discoveries of two-dimensional (2D) Dirac materials in which the quasiparticles are governed by relativistic quantum mechanics, especially the experimental separation of graphene [7–13], made it possible to realize the phenomenon of atomic collapse in experiments. Specifically, the Fermi velocity in graphene is two orders of magnitude smaller than the speed of light: $v_F \sim 10^6 m/s$, so the effective fine structure constant for graphene is on the order of unity. The critical value of the nuclear charge for atomic collapse in a graphene "environment" then becomes $Z_c \approx 1$. This means that graphene would significantly enhance the relativistic quantum effects of any ordinary atom placed within, rendering possible experimental observation of atomic collapse [14,15]. Previous theoretical work investigated various physical behaviors associated with the discrete and continuum energy states of an atomic impurity placed in graphene before and after atomic collapse, which include screening [16,17], density of states [14,15,18,19], scattering phase [15,20], and generalization, taking into account electron-electron interaction [21].

The first experimental observation [22,23] of atomic collapse in graphene was achieved in 2012/2013. A tunable artificial atom in graphene was subsequently experimentally realized [24]. Recently, it has been shown that atomic collapse states can be induced by an STM-tip [25], and a scale anomaly

*Ying-Cheng.Lai@asu.edu

together with a universal quantum phase transition has been observed [26].

The past few years have witnessed a growing interest in relativistic quantum, pseudospin-1 quasiparticles that can arise in T_3 or dice lattices [27–57]. The T_3 lattice structures were first discussed [58] in 1986, which can be constructed by altering the honeycomb lattice structure (e.g., of graphene) to include an additional atom at the center of each hexagon, leading to an energy band structure that constitutes a pair of Dirac cones and a flat band with a conical intersection of triple degeneracy. As a result, three independent spinor components are required to describe the system, making the quasiparticles effectively pseudospin-1. Theoretically, pseudospin-1 quasiparticles are described by the generalized Dirac-Weyl equation [27,28,47]. In recent studies, the scattering of pseudospin-1 quasiparticles from a circular step potential [48,55] and their magnetic properties [59] have been investigated. There has also been work on the transport properties (e.g., conductivity) of pseudospin-1 quasiparticles in the presence of atomic impurities [35,43,56] as well as on plasmons and screening in the pseudospin-1 dice lattice [60]. While an electronic T_3 lattice has not been realized in experiments yet, theoretical and computational studies revealed that pseudospin-1 quasiparticles can arise in photonic lattices [31,61–63] and this has been verified in a recent experiment [64].

The interest in and the gradual development of the physics of pseudospin-1 quasiparticles has motivated us to ask the fundamental question of whether atomic collapse can occur in such systems. In this paper, we address this question by analytically solving the Dirac-Weyl equation underlying the pseudospin-1 relativistic quantum system in the presence of a Coulomb potential field. Our approach is to focus on the continuum limit where the solutions of the Dirac-Weyl equation can be obtained through a decoupling method. Analyzing the solutions yields a simple but general criterion for the occurrence of atomic collapse in terms of the normalized strength of Coulomb interaction and the angular momentum quantum number. Remarkably, we find that, for the lowest angular momentum state, the solution coincides with that for pseudospin-1/2 systems, confirming unequivocally the possibility of atomic collapse in pseudospin-1 systems. For higher angular momentum states, the pseudospin-1 wave functions exhibit a singularity at the zero kinetic energy point. The divergence of the local density of states (LDOS) associated with the flat band leads to an inverse square type of singularity in the conductivity. These findings provide basic insights into the physics of the two-body, relativistic quantum pseudospin-1 systems. The problem of atomic collapse not only is fundamental to relativistic quantum mechanics, but also has implications on the development of devices based on 2D Dirac materials in view of the inevitable and ubiquitous presence of atomic impurities.

II. SOLUTION OF DIRAC-WEYL EQUATION FOR PSEUDOSPIN-1 PARTICLES IN A COULOMB POTENTIAL FIELD

The 2D lattice structure and the underlying energy band structure of a pseudospin-1 system in the presence of a Coulomb impurity are shown in Fig. 1. In the unit $\hbar = 1$, the

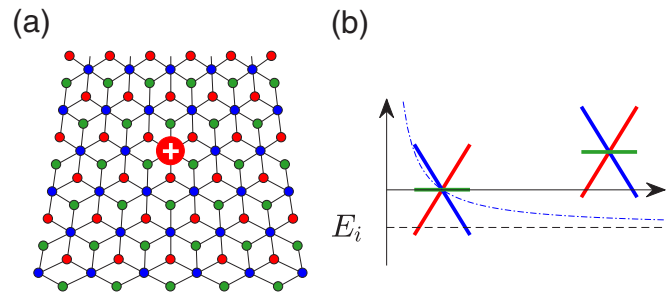

FIG. 1. *Pseudospin-1 lattice and energy band structure*. (a) A pseudospin-1 lattice where the three sublattices of nonequivalent atoms are distinguished by color (red, blue, and green, respectively). A Coulomb impurity is shown as the red cross. (b) Energy band structure in the presence of the impurity scattering atom. At each point, the energy band constitutes a pair of Dirac cones and a flat band through the conic intersecting point. Because of the Coulomb potential, locally the height of the three-band structure depends on the position. The black and blue dashed lines indicate the energy E_i of the incident particle and the kinetic energy $E - V$, respectively.

Hamiltonian is given by

$$H = v_F \boldsymbol{S} \cdot \boldsymbol{p} - \frac{Ze^2}{\kappa r}, \tag{1}$$

where v_F is the Fermi velocity, $\boldsymbol{p} = (p_x, p_y)$ is the momentum or wave vector, and $\boldsymbol{S} = (S_x, S_y)$ are two 3×3 matrices which, together with another 3×3 matrix S_z, constitute the "generalized" Pauli matrices that form a complete representation of spin one. The three matrices are given by

$$S_x = \frac{1}{\sqrt{2}} \begin{pmatrix} 0 & 1 & 0 \\ 1 & 0 & 1 \\ 0 & 1 & 0 \end{pmatrix}, \quad S_y = \frac{1}{\sqrt{2}} \begin{pmatrix} 0 & -i & 0 \\ i & 0 & -i \\ 0 & i & 0 \end{pmatrix},$$
$$S_z = \begin{pmatrix} 1 & 0 & 0 \\ 0 & 0 & 0 \\ 0 & 0 & -1 \end{pmatrix}, \tag{2}$$

which satisfy the angular momentum commutation relations $[S_l, S_m] = i\epsilon_{lmn} S_n$ with three eigenvalues: $s = \pm 1, 0$, where ϵ_{lmn} is the Levi-Civita symbol. It is convenient to introduce two normalized parameters: $g = Ze^2/\kappa v_F$ and $\varepsilon = E/v_F$, to characterize the strength of the Coulomb field and the energy scale, respectively. It is also convenient to set the radial variable in polar coordinates (ρ, θ) as $\rho \equiv \varepsilon r$. Depending on the sign of Z, the value of g can be either positive or negative [14–21]. In the tight-binding approximation, the Fermi velocity is given by $v_F = 3at/\sqrt{2}$, where a is the lattice constant and t is the nearest-neighbor hopping energy of the hexagonal lattice [27].

We aim to solve the eigenvalue problem,

$$H\boldsymbol{\psi} = E\boldsymbol{\psi}, \tag{3}$$

with the three-component spinor $\boldsymbol{\psi} = (\psi_1, \psi_2, \psi_3)^T$. Because of the circular symmetry of the Coulomb potential field, the angular momentum l is a good quantum number, making it useful to write the spinor in terms of the angular-momentum

eigenstate $e^{il\theta}$ as

$$\boldsymbol{\psi} = \frac{1}{2\sqrt{2\pi}} \begin{pmatrix} \psi_A e^{-i\theta} \\ \sqrt{2} i \psi_B \\ -\psi_C e^{i\theta} \end{pmatrix} e^{il\theta}, \tag{4}$$

where $l = 0, \pm 1, \cdots$. In the angular-momentum representation, Eq. (3) becomes

$$\begin{pmatrix} \rho + g & -r\partial_r - l & 0 \\ r\partial_r - l + 1 & 2(\rho + g) & -r\partial_r - l - 1 \\ 0 & r\partial_r - l & \rho + g \end{pmatrix} \begin{pmatrix} \psi_A \\ \psi_B \\ \psi_C \end{pmatrix} = 0, \tag{5}$$

which can be solved by using a decoupling method (Appendix A). The result for component ψ_B is

$$\psi_B = (\rho/g)^{-1/2+s} \exp(i\rho)\phi_B, \tag{6}$$

where

$$s = \sqrt{\tfrac{1}{4} - (g^2 - l^2)} \tag{7}$$

and ϕ_B is given by

$$\phi_B = A \cdot \mathrm{HeunC}(\alpha, \beta, \gamma, \delta, \eta, -\rho/g), \tag{8}$$

with A being the normalization constant that can be obtained through the asymptotic behavior of ϕ_B, and HeunC denotes the confluent Heun function which, in some special cases, can be related to the hypergeometric function [65–67]. The five parameters are

$$\begin{aligned} \alpha &= -2ig, \\ \beta &= 2s, \\ \gamma &= -2, \\ \delta &= -2g^2, \\ \eta &= 2g^2 + 3/2. \end{aligned} \tag{9}$$

The other two components, ψ_A and ψ_C, can be expressed in terms of ψ_B:

$$\begin{aligned} \psi_A &= \frac{r\psi_B' + l\psi_B}{\rho + g}, \\ \psi_C &= \frac{-r\psi_B' + l\psi_B}{\rho + g}, \end{aligned} \tag{10}$$

which can be calculated by using the derivative property of the confluent Heun function [68].

III. ATOMIC COLLAPSE STATES IN PSEUDOSPIN-1 SYSTEMS

To gain insights into the possible occurrence of atomic collapse in pseudospin-1 systems, we examine some special cases. One such case is the lowest angular momentum state $l = 0$. In Appendix B, we show that this state is identical to the lowest angular momentum state in the corresponding pseudospin-1/2 system. For $l \neq 0$, the solutions of the $+l$ and $-l$ states are identical except for a normalization constant. Another special case is the spatial location defined by $\rho + g = 0$. At this point, the determinant of Eq. (5) is zero—which is characteristic of the solution associated with the flat band. This is a special feature of pseudospin-1 systems, which does not arise in the corresponding pseudospin-1/2 systems. The physical meaning of this solution is that it corresponds to the point at which the kinetic energy is zero: $E - V(r) = 0$. We will show later that, at the zero kinetic energy point, the wave function exhibits a singularity of the form $[E - V(r)]^{-1}$. At this point, the solutions associated with the conic bands and the flat band are degenerate.

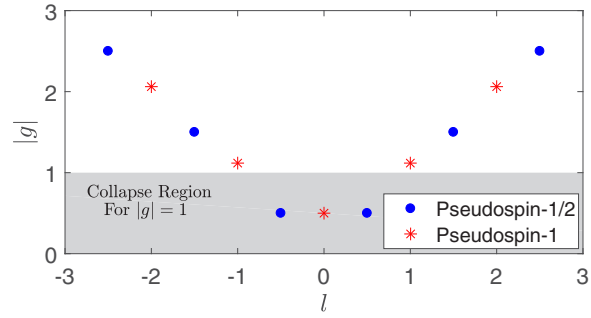

FIG. 2. *Possible atomic collapse states for pseudospin-1 and pseudospin-1/2 systems*. As the strength $|g|$ of the Coulomb impurity is increased, more and more collapse states are possible, each associated with a distinct angular momentum number. For pseudospin-1 systems, the second spinor component can be conveniently used to find the collapse states. For pseudospin-1/2 systems, the condition under which atomic collapse occurs is that the quantity $s = \sqrt{l^2 - g^2}$ becomes imaginary, where l is the angular momentum quantum number associated with the first spinor component plus 1/2. Atomic collapse states can arise but only for $|g| > 1/2$. For example, for $1/2 < |g| \leqslant 1$, the shaded region indicates that there is only one collapse state for a pseudospin-1 system, which occurs at $l = 0$, but for a pseudospin-1/2 system, two such states exist: $l = \pm 1/2$.

In general, the asymptotic (far field) behavior of ψ_B is governed by the Whittaker equation. Our analysis (Appendix B) reveals that ψ_B contains the phase shift $\log|\rho|$ and is given by

$$\psi_B \sim \sqrt{\frac{2}{\pi r}} \cos\left[|\rho| + \tilde{g}\log(2|\rho|) + \delta_l\right], \tag{11}$$

where $\tilde{g} = \mathrm{Sign}(\varepsilon)g$ and δ_l is the scattering phase associated with the angular momentum l. The $\sqrt{1/r}$ decay factor stipulates that there are no bound states for massless particles in the pseudospin-1 system in the presence of a Coulomb impurity, similar to the situation in the corresponding pseudospin-1/2 systems [14–21]. Physically, this means that the minimum energy occurs at infinity.

Can atomic collapse occur in pseudospin-1 systems? As previously demonstrated for pseudospin-1/2 systems [14,18], an atomic collapse state arises when the quantity s in Eq. (7) becomes imaginary. In particular, since the wave function near the impurity behaves as $r^{-1/2+s} = r^{-1/2}\exp(s\log r)$, an imaginary s will lead to an infinite number of nodes in the wave function for $r \to 0$. Atomic collapse can then be expected to occur in pseudospin-1 systems. A difference between the two types of systems lies in the number of the collapse states. Figure 2 shows, for both types of systems, the possible collapse states in the parameter plane $(l, |g|)$. For example, for $|g| = 1$, the only state of atomic collapse for the pseudospin-1 system is $l = 0$, whereas there are two collapse states for the pseudospin-1/2 system, which

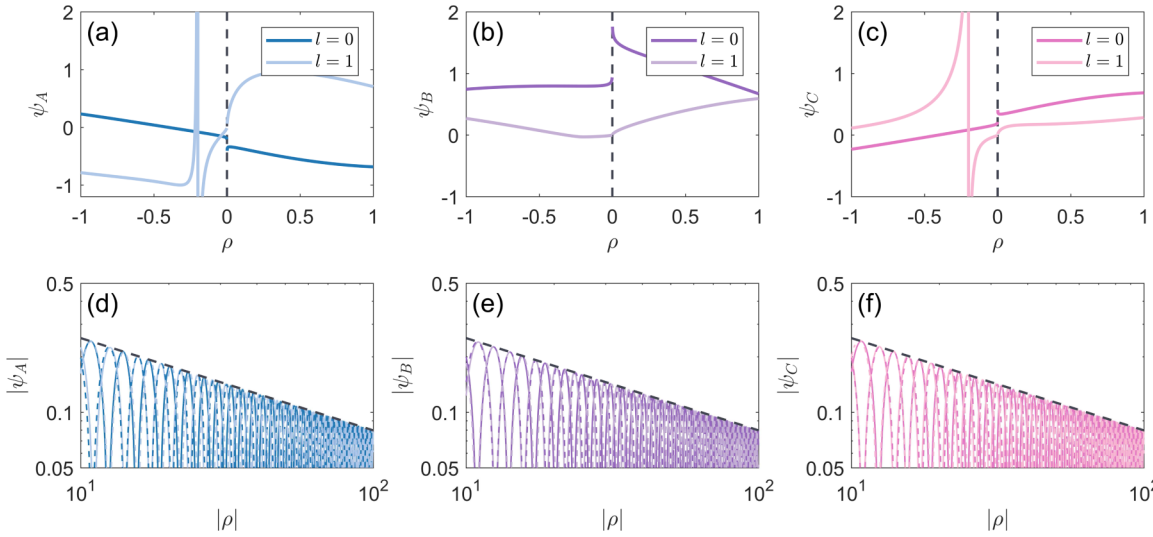

FIG. 3. *Scattering wave function in the collapse-free regime*. For $g = 1/5$, (a) spinor component ψ_A, where the vertical dashed line denotes $r = 0$. As indicated by Eq. (6), in this regime the Coulomb impurity will generate a singularity. (b), (c) Spinor components ψ_B and ψ_C, respectively. The singularity at $\rho = -g$ is a result of the flat band. In the presence of an impurity, the solutions associated with the flat band and with the Dirac cones are mixed. In terms of the angular momentum, the singularity occurs for $l \neq 0$. (d)–(f) The absolute values of ψ_A, ψ_B and ψ_C, respectively for $|\rho| \gg 1$, where each color dashed line indicates the wave-function component for negative values of ρ. The dashed black envelope line is indicative of the decay behavior $\sqrt{2/(\pi r)}$ given by Eq. (11).

occur at $l = \pm 1/2$. For certain boundary condition, the two atomic collapse states can be degenerate [14,15]. An analysis of the issue of broken degeneracy between the $\pm l$ states in pseudospin-1/2 and pseudospin-1 systems is given in Appendix C.

For a strong impurity, s becomes an imaginary number for some state l. We thus have an additional set of linearly independent solutions:

$$\phi_B = C_1 \mathrm{HeunC}(\alpha, \beta, \gamma, \delta, \eta, -\rho/g) + C_2(-\rho)^{-\beta}\mathrm{HeunC}(\alpha, -\beta, \gamma, \delta, \eta, -\rho/g), \quad (12)$$

where C_1 and C_2 are two parameters that can be determined by the boundary and normalization conditions. Other parameters in Eq. (12) are the same as those in Eq. (9). Numerically, the confluent Heun function can be evaluated through its integral representation [65].

A. Collapse-free regime: Weak impurity ($|g| < 1/2$)

In general, the behaviors of the wave functions in the collapse-free and collapse-prone regimes can be quite different, as in graphene systems [14,15]. For pseudospin-1 systems, the separation between the two regimes is at $|g| = 1/2$, as shown in Fig. 2. Especially, for $|g| < 1/2$, no collapse state is possible, where s takes on real values for all the states. In this case, the solution is given by Eq. (6), which involves only one set of confluent Heun functions.

For a pseudospin-1 system in free space, the spinor solution has nonzero values only for the first and third components (ψ_A and ψ_C)—the second component ψ_B is zero due to the flat band. When an impurity is introduced into the system, the three components will be mixed. The flat band can lead to a singularity in the spinor components. For a Coulomb impurity, ψ_A and ψ_C both will possess a singularity, and ψ_B will become nonzero but without any singularity. Figure 3 shows the three spinor components for both positive and negative values of ρ. As shown in Figs. 3(a) and 3(c) for ψ_A and ψ_C, respectively, a singularity arises at $\rho + g = 0$. This can be seen by noting from Eq. (5) that, at the zero kinetic energy point determined by $\rho + g = 0$, the corresponding matrix has zero determinant, leading to a singularity [69]. Analytically, we are able to show that the singularity leads to a $[E - V(r)]^{-1}$ type of asymptotic behavior in the region where the kinetic energy is about zero, as detailed in Appendix B. Such a singularity occurs in pseudospin-1 systems with three spinor components. In contrast, a pseudospin-1/2 system does not have this type of singularity, as the determinant of the corresponding 2×2 matrix has a nonzero value. Note also that, for $l = 0$, the spinor solutions of pseudospin-1 and pseudospin-1/2 systems are identical. Thus, for pseudospin-1 systems, this type of singularity arises for $l \neq 0$ only.

Figures 3(d)–3(f) show the far-field behaviors of the three spinor components, which all exhibit a $1/\sqrt{r}$ type of decay, as predicted by the far-field approximation in Eq. (11). There thus exists no bound state, as for pseudospin-1/2 systems. In fact, because of the massless nature of the quasiparticles, no bound state can form with any finite potential confinement. The distinct feature in pseudospin-1 systems is the emergence of some singular behavior at a finite distance.

To further characterize the wave-function behaviors of pseudospin-1 systems in the presence of an impurity, we examine the LDOS defined as

$$N(\varepsilon, r) = \frac{1}{8\pi}\sum_l (|\psi_A|^2 + 2|\psi_B|^2 + |\psi_C|^2), \quad (13)$$

where the factor of two in front of $|\psi_B|^2$ comes from the factor of $\sqrt{2}$ associated with the second spinor component in Eq. (4). In the low-energy regime, the expression in Eq. (13) is truncated for a finite value of the angular momentum l.

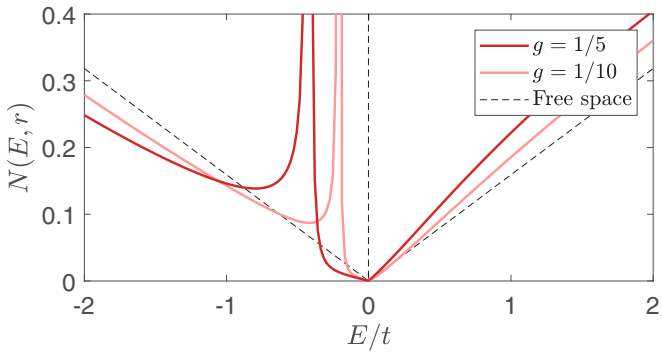

FIG. 4. *Local density of states (LDOS) of pseudospin-1 systems in the collapse-free regime*. Shown are patterns of LDOS at the location $r = a$, for different values of g. The dashed lines indicate the free space DOS where $N(E, r) = |E|/(2\pi)$ and $N(0) = \infty$.

As shown in Fig. 4, the LDOS diverges at $\rho + g = 0$, as the square term in the LDOS gives

$$\lim_{E\to V(r)} \sigma(r) \sim (E - E_0)^{-2}, \tag{14}$$

where $\sigma(r)$ is the conductivity that depends on r and E_0 with the latter defined as

$$\frac{E_0}{t} \equiv -\frac{3}{\sqrt{2}}\frac{a}{r}g. \tag{15}$$

For a positive value of g (an impurity with a positive charge), the singularity occurs in the negative energy domain. In an experiment, a positively charged impurity can be generated by introducing an ion (e.g., Co^+ or Ca^+) into the system, and the DOS can be measured through the conductivity [22,23]. Especially under a negative bias, one can use an STM tip at some distance to assess the zero kinetic energy point with divergent conductivity. For a pure pseudospin-1 lattice, the flat band does not have any contribution to conductivity. However, under the nonequilibrium condition [56] or when an impurity is present, the flat band can contribute significantly to conductivity. Here, our analysis of the infinite lattice shows that a Coulomb impurity can shift the energy and lead to a $(E - E_0)^{-2}$ type of divergence in conductivity.

B. Collapse-prone regime: Strong impurity ($|g| > 1/2$)

A pseudospin-1 system is prone to atomic collapse in the strong impurity regime characterized by $|g| > 1/2$. For a collapse state, the value of s in Eq. (12) is imaginary, corresponding to $l^2 < g^2 - 1/4$. In this case, the second spinor component ϕ_B contains an additional linearly independent solution. (Note that the additional solution does not arise for a noncollapse state because of the real values of s).

In quantum electrodynamics, atomic collapse stipulates that a bound state be replaced by a state with particle-hole generation [3]. However, for massless quasiparticles in 2D Dirac materials, there is no bound state and an atomic collapse is manifested through the strong impurity-induced infinite oscillations of the wave function for $r \to 0$, which is related to the phenomenon of Landau fall [14,18,70]. To detect the infinite number of oscillations, we truncate the solution by introducing an interior boundary condition. Following Refs. [14,18,71], we truncate the spinor wave function at an infinitesimal distance to generate a forbidden region into which the particle cannot enter. The truncation can typically be viewed as introducing an infinite mass potential near the impurity by setting zero the current across the boundary. This is effectively a screening effect that makes the real potential deviate from the Coulomb potential but only for $r \to 0$.

We set up the boundary conditions as follows. In polar coordinates, the current components in a pseudospin-1 system [48] are

$$\begin{aligned} j_r &= v_F \boldsymbol{\psi}^\dagger \mathbf{S}\cdot\hat{e}_r\boldsymbol{\psi} = \sqrt{2}\mathrm{Re}[\psi_2^*(\psi_1 e^{i\theta} + \psi_3 e^{-i\theta})], \\ j_\theta &= v_F \boldsymbol{\psi}^\dagger \mathbf{S}\cdot\hat{e}_\theta\boldsymbol{\psi} = -\sqrt{2}\mathrm{Im}[\psi_2^*(\psi_1 e^{i\theta} - \psi_3 e^{-i\theta})]. \end{aligned} \tag{16}$$

Imposing the constraint $j_{a_0} = 0$ and utilizing the spinor wave function expression in Eq. (4), we get

$$2\psi_B(a_0) = \psi_A(a_0) - \psi_C(a_0). \tag{17}$$

For $l = 0$, we have $\psi_A = -\psi_C$ and Eq. (17) gives $\psi_A(a_0) = \psi_B(a_0)$, which has the same form as the boundary condition in a pseudospin-1/2 system. However, for $l \neq 0$, the equivalent relation does not hold. Using Eq. (17) and the normalization condition for $r \to \infty$, we can obtain the coefficients C_1 and C_2 in Eq. (12). For the modes that do not exhibit any collapse behavior, the solutions have the same form as those in the collapse-free regime.

In the collapse-prone regime, the LDOS contains two types of contributions:

$$N(E, r) = \sum_{l^2<g^2-1/4} \bar{n}_l(E, r) + \sum_{l^2>g^2-1/4} n_l(E, r), \tag{18}$$

where $\bar{n}_l$ denotes the contribution of the collapse state that has two linearly independent solutions. Figure 5(a) shows the LDOS for $g = 1$. From Eq. (7), we see that, for this impurity strength, the $l = 0$ state can collapse. Figure 5(a) reveals a singularity in the LDOS in the regime of negative impurity strength, which is a consequence of the flat band, as in the collapse-free regime discussed in Sec. III A. Another singularity occurs for $E \to 0^-$. The rapid oscillations in this energy range are characteristic of an atomic collapse state, as can be better seen on a logarithmic scale in Fig. 5(b). There is then atomic collapse for the $l = 0$ state in the pseudospin-1 system.

Comparing with the collapse state in pseudospin-1/2 systems, the density for oscillation peaks in pseudospin-1 systems is reduced, as caused by a decrease in the number of collapse states. The oscillatory behavior in the LDOS also occurs in the positive energy range, as shown in Fig. 5(c), where the correction $\delta N = N_{g=1} - N_{g=0}$ to the LDOS is displayed. We note that similar oscillation patterns have been observed in pseudospin-1/2 systems [14,18,72].

C. Divergence in conductivity associated with Coulomb impurity

A unique phenomenon in pseudospin-1 systems, which does not arise in pseudospin-1/2 systems, is flat-band-induced divergence of conductivity. A previous study based on the random phase approximation method [60] showed that the flat band leads to a single point of divergence. There was also a discussion about conductivity divergence induced by

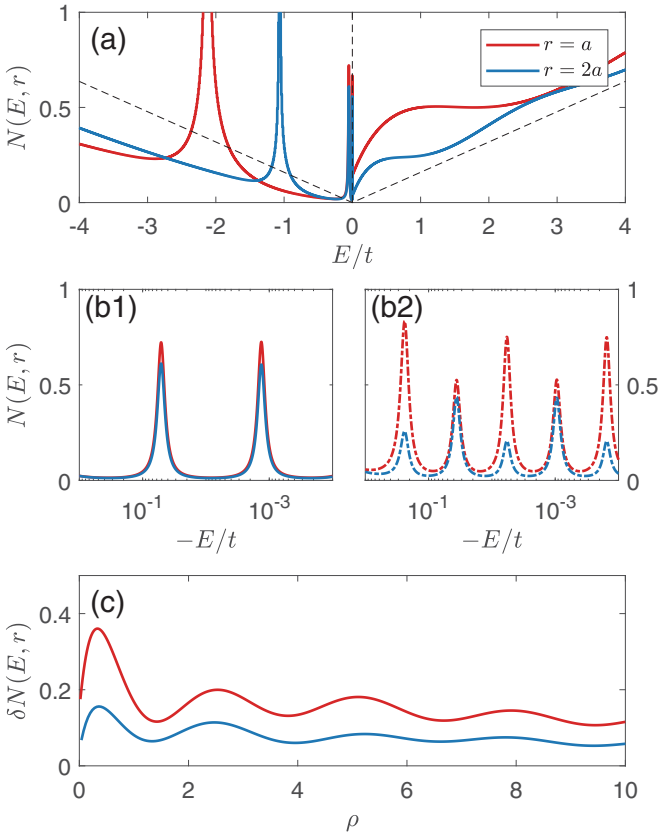

FIG. 5. *Local density of states (LDOS) of a pseudospin-1 system in the collapse-prone regime*. For $g = 1$ and truncation at $a_0 = 0.5a$ (a) LDOS for different values of r where the rapid oscillations near $E \to 0^-$ are indicative of atomic collapse, (b1) LDOS for the zero angular momentum ($l = 0$) mode on a logarithmic energy scale and (b2) LDOS for the $l = \pm 1/2$ modes for the corresponding pseudospin-1/2 system. (c) Oscillatory behavior in the LDOS difference $\delta N = N_{g=1} - N_{g=0}$—a signature of atomic collapse.

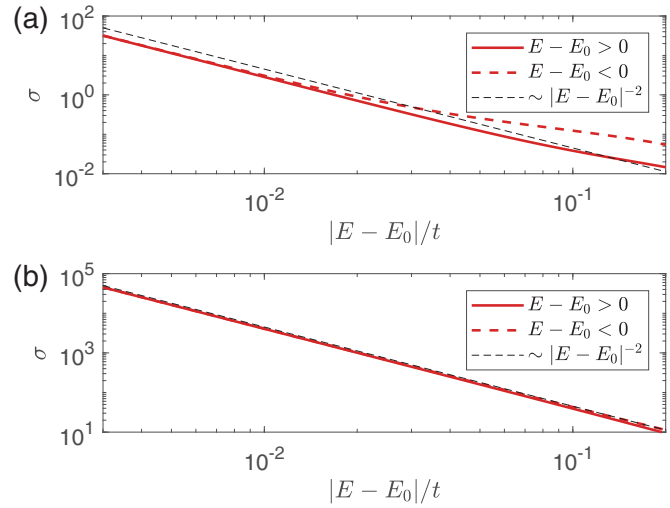

FIG. 6. *Flat-band induced divergence of conductivity in pseudospin-1 systems*. (a) Shown is the behavior of LDOS near E_0 for $g = 1/5$ and $r = a$, where $E_0 = -3t/(5\sqrt{2}) \approx -0.42t$ [Eq. (15)]. There is a singularity in the spinor wave function determined by $\rho + g = 0$ [or, equivalently, $E - V(r) = 0$]. In this case, the LDOS and hence the conductivity exhibits a $(E - E_0)^{-2}$ type of divergence as the energy approaches E_0. (b) The same quantity for $g = 1$.

impurities [35]. We wish to point out that the analytical solution of the Dirac-Weyl equation gives directly the point of divergence in conductivity. As shown in Fig. 6, as the kinetic energy $E - V(r)$ tends to zero, the conductivity diverges. In fact, in this energy regime, the conductivity scales with the energy difference as $(E - E_0)^{-2}$.

For screening at a constant position, the resonant width is proportional to the impurity strength. Since the system is invariant with respect to ϵr, screening near the impurity implies broadening of the energy region, as shown in Fig. 5(a). If screening is done at infinity, the peak width and position will be the same as those in the free space.

We examine the spatial distribution of the wave function associated with divergent conductivity. For a given value of the incident energy, we can get the zero kinetic energy point from Eq. (15). In the centrally symmetric coordinate system, we can calculate the current components in the radial and angular directions, j_r and j_θ, respectively (Appendix B). A phenomenon of interest is that the current is discontinuous in the angular direction for a noncollapse state, as shown in Fig. 7. In fact, for a pseudospin-1 system, the current components are $j_r = 0$ and $j_\theta \propto 1/(r - r_0)$ for the $l \neq 0$ states in the noncollapse regime. This discontinuous behavior does not arise in pseudospin-1/2 systems where the angular current component is continuous. The reason is that the currents associated with a particle and a hole on the two sides of the boundary have different directions. However, for plane-wave scattering, all angular momentum channels are mixed. As a result, in the collapse-free region, the time reversal symmetry $l \to -l$ stipulates a zero net current.

IV. DISCUSSION

The intriguing relativistic quantum phenomenon of atomic collapse cannot occur for ordinary systems because of the unrealistically high value of the atomic number required, i.e., it should be larger than the inverse of the fine structure constant. However, in solid-state materials that host relativistic quantum quasiparticles, due to the two-order-of-magnitude reduction in the "speed of light" (e.g., in graphene, the Fermi velocity is typically 100 times smaller than the speed of light in vacuum), the effective fine-structure constant is on the order of unity. As a result, in principle, an impurity of any number of protons can induce atomic collapse. Previously, the possibility of realizing atomic collapse in graphene was theoretically articulated [14–21] and experimentally investigated [22–24,26]. Beyond graphene, other types of relativistic quantum solid-state materials that have attracted growing interest in recent years are those which host pseudospin-1 quasiparticles, whose energy band structure consists of a pair of Dirac cones and a flat band [27–57]. A natural question is whether atomic collapse can occur in pseudospin-1 material systems.

We have addressed this question by using the setting of a Coulomb impurity embedded in a pseudospin-1 lattice and

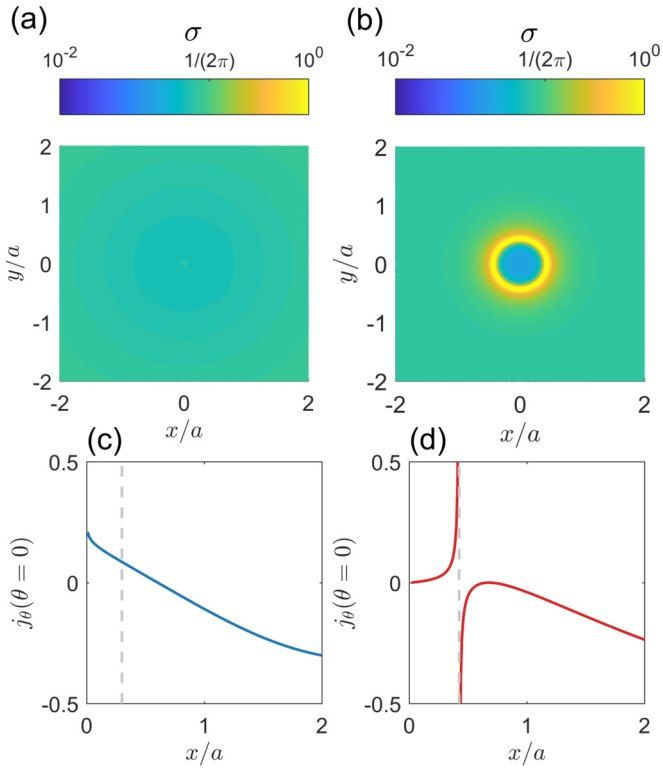

FIG. 7. *Comparison between pseudospin-1/2 and pseudospin-1 systems*. The parameters are $E = -t$ (constant bias) and $g = 1/5$. (a) Conductivity for a pseudospin-1/2 system, where space is in units of the atomic lattice spacing a. The values of the conductivity are color coded on a logarithmic scale with $1/(2\pi)$ being the free space conductivity. (b) Conductivity for a pseudospin-1 system, where the legends are the same as in (a). (c) Current in the pseudospin-1/2 system associated with the $l = 1/2$ state, where $j_r = 0$ and j_θ is continuous when passing through the zero kinetic energy region (dashed line). (d) Current in the pseudospin-1 system associated with the $l = 1$ state, where j_θ changes sign when passing through the zero kinetic energy region at which the value of the current diverges.

obtained analytic expressions of the spinor wave functions. Our main result is that, for normalized Coulomb impurity strength g and a state with the angular momentum quantum number l, the general condition under which atomic collapse can occur is

$$l^2 < g^2 - 1/4. \tag{19}$$

Thus, the critical impurity strength above which atomic collapse can occur is $|g| = 1/2$, which is identical to that in graphene. Furthermore, we have shown that, for the lowest angular momentum state $l = 0$, the wave-function solution associated with atomic collapse has the same form as that in a pseudospin-1/2 system, but with a reduced number of states. Distinct solutions from those in graphene arise only for nonzero angular momentum states ($l \neq 0$).

In general, the relativistic quantum motion of a higher spin particle can be treated as a few-body problem of particles with a lower spin value. For example, a pseudospin-1 particle is equivalent to two pseudospin-1/2 particles, where the wave function of the former can be written as the direct product of the wave functions of the latter. In the central mass coordinate, the Hamiltonian of the two pseudospin-1/2 particles is equivalent to that of a pseudospin-1 particle [69,73]. In fact, the two-body system is one of the solvable problems in relativistic quantum mechanics [74], whose solution provides great insights into many-body behaviors in graphene [21,75]. Following this idea, we have obtained the result demonstrating that a pseudospin-1 system in the presence of a Coulomb potential is completely equivalent to a two-body system of pseudospin-1/2, because two such particles will naturally generate a Coulomb interaction. (In Appendix D, we show that, by constructing a direct product of the wave functions, a relativistic quantum two-body system and a pseudospin-1 system subject to a Coulomb impurity have similar solution forms).

A possible way to gain insights into the collapse state in a pseudospin-1 lattice is then to study the exciton in graphene where conductivity divergence is expected. Indeed, we have found the divergent behavior in pseudospin-1 systems.

In high-energy physics, the bound states of a massive spin-1 particle subject to a magnetic field were studied and the differences from those of spin-1/2 particles were noticed [76–78]. Theoretically, relativistic spin-1 particles can also be described by the Duffin-Kemmer-Petiau (DKP) equation [79]. In the presence of a Coulomb impurity, the DKP equation is reduced to the Heun equation [80]. We also note that, in the standard model, a spin-1 field can express gluons, photons, W and Z bosons. They are real particles but their Lagrangian involves four components to satisfy the Lorentz invariance. Besides, real spin-1 particles cannot form a bound state. On the other hand, the DKP equation similar to the Dirac equation but with ten components. To our knowledge, both the standard and the DKP models have no relationship with pseudospin-1 systems that have three spinor components.

At the present time, lattice systems hosting pseudospin-1 particles have not been experimentally realized. If such a lattice is synthesized in the near future, it would be possible to observe the phenomenon of atomic collapse, as suggested by our work. In particular, the Coulomb impurity has been experimentally implemented in graphene systems [22–24,26], and it is not unreasonable to expect that the technique can be carried over to pseudospin-1 systems. For a positive ion in a pseudospin-1 lattice under a negative bias, the STM technique can be used to detect atomic collapse through conductivity divergence that occurs at the point of zero kinetic energy.

Extensions of the present work are possible. For example, an experimentally relevant issue is STM-tip-induced collapse. Particularly, instead of using charged dimers, a sharp STM tip can also induce atomic collapse, which is more accessible to experiments and more tunable. Another issue is the finite size effects. With the exact solutions of the wave functions, it should be possible to study finite size effects analytically by applying the correct boundary conditions (e.g., zigzag or infinite mass) [81]. This enables a study of the individual states, potentially leading to more detailed information about the atomic collapse states. A magnetic field could give the same information, although it may not be feasible to obtain exact analytical solutions of the Dirac equation in the simultaneous presence of a Coulomb potential and a magnetic field.

ACKNOWLEDGMENTS

We would like to acknowledge support from the Vannevar Bush Faculty Fellowship program sponsored by the Basic Research Office of the Assistant Secretary of Defense for Research and Engineering and funded by the Office of Naval Research through Grant No. N00014-16-1-2828. D.H. is supported by the DoD LUCI (Lab-University Collaborative Initiative) Program.

APPENDIX A: ANALYTICAL SOLUTION OF ψ_B

From Eq. (1), we obtain the eigenstate problem:

$$\frac{v_F}{\sqrt{2}}\left(-i\boldsymbol{S}\cdot\nabla-\frac{\sqrt{2}g}{r}\right)\boldsymbol{\psi}=E\boldsymbol{\psi}. \tag{A1}$$

The eigenstate equation can be reduced to the following matrix equation:

$$\frac{1}{\sqrt{2}}\begin{pmatrix}-\sqrt{2}(\varepsilon+g/r) & \hat{L}_- & 0\\ \hat{L}_+ & -\sqrt{2}(\varepsilon+g/r) & \hat{L}_-\\ 0 & \hat{L}_+ & -\sqrt{2}(\varepsilon+g/r)\end{pmatrix}\times\begin{pmatrix}\psi_A e^{i(l-1)\theta}\\ \sqrt{2}i\psi_B e^{il\theta}\\ -\psi_C e^{i(l+1)\theta}\end{pmatrix}=0, \tag{A2}$$

where

$$\hat{L}_\pm=-ie^{\pm i\theta}\left(\partial_r\pm i\frac{\partial_\theta}{r}\right). \tag{A3}$$

Inserting $\hat{L}_\pm$ to separate the angular part, we get Eq. (5), where the first and the third spinor components, ψ_A and ψ_C, respectively, are given by

$$\begin{aligned}\psi_A&=\frac{r\psi_B'+l\psi_B}{\varepsilon r+g},\\ \psi_C&=\frac{-r\psi_B'+l\psi_B}{\varepsilon r+g}.\end{aligned} \tag{A4}$$

Introducing $R=\varepsilon r/g$, we have

$$\psi_B''+\frac{R+2}{R(R+1)}\psi_B'+\left(g^2+\frac{2g^2}{R}+\frac{g^2-l^2}{R^2}\right)\psi_B=0. \tag{A5}$$

This equation has two second-order singularities at $R=0$ and ∞, respectively. Following the method in Ref. [14], we can eliminate the second-order singularities. First consider the singularity at $R\to 0$. Using

$$\lim_{R\to 0}\psi_B\sim R^x \tag{A6}$$

and omitting the term that contains R, we get the equation for $x=-1/2+s$. Similarly, for the singularity at $R\to\infty$, we have $\psi_B\sim e^{igR}$. We thus consider

$$\psi_B=R^{-1/2+s}e^{igR}\phi_B. \tag{A7}$$

Inserting this into Eq. (A5) and making the change $\mathcal{R}=-R$, we get the following second-order differential equation:

$$\phi_B''+\left(\frac{2s+1}{\mathcal{R}}-\frac{1}{\mathcal{R}-1}-2ig\right)\phi_B'+\left(\frac{-\mathcal{R}(2g^2+2igs)+(s-ig)(2ig-1)+1/2}{\mathcal{R}(\mathcal{R}-1)}\right)\phi_B=0. \tag{A8}$$

From Refs. [65] and [82], we have that the standard form of the confluent Heun equation is

$$\frac{d^2y}{dz^2}+\left(\alpha+\frac{\beta}{z}+\frac{\gamma+1}{z-1}\right)\frac{dy}{dz}+\left(\frac{\nu}{z-1}+\frac{\mu}{z}\right)y=0, \tag{A9}$$

where

$$\begin{aligned}\mu&=\tfrac{1}{2}[\alpha-\beta-\gamma-2\eta+\beta(\alpha-\gamma)],\\ \nu&=\tfrac{1}{2}[\alpha+\beta+\gamma+2\delta+2\eta+\gamma(\alpha+\beta)].\end{aligned} \tag{A10}$$

Comparing Eq. (A8) with Eq. (A9), we can get each parameter for the confluent Heun equation. For noninteger values of β, another linearly independent solution is $z^{-\beta}\mathrm{HeunC}(\alpha,-\beta,\gamma,\delta,\eta,z)$.

APPENDIX B: SPECIAL CASES

1. Zero angular momentum state

For $l=0$, Eq. (5) is reduced to

$$\begin{aligned}\psi_A+\psi_C&=0,\\ r\psi_A'+\psi_A+(\varepsilon r+g)\psi_B&=0,\\ r\psi_B'-(\varepsilon r+g)\psi_A&=0.\end{aligned} \tag{B1}$$

where the second and third equations can be regarded as describing a pseudospin-1/2 particle under a Coulomb potential:

$$\begin{pmatrix}-\varepsilon-g/r & \hat{L}_-\\ \hat{L}_+ & -\varepsilon-g/r\end{pmatrix}\begin{pmatrix}\psi_A e^{-i\theta}\\ i\psi_B\end{pmatrix}=0. \tag{B2}$$

2. The case of $\rho+g=0$

The relationship between ψ_A and ψ_C implies a singularity at $\varepsilon r+g=0$:

$$\begin{aligned}\psi_A&=\frac{r\psi_B'+l\psi_B}{\varepsilon r+g},\\ \psi_C&=\frac{-r\psi_B'+l\psi_B}{\varepsilon r+g}.\end{aligned} \tag{B3}$$

An alternative way is to examine the $l\neq 0$ state by separating ψ_A and ψ_C. Specifically, introducing

$$\begin{aligned}\psi_A-\psi_C&=F,\\ \psi_A+\psi_C&=G,\end{aligned} \tag{B4}$$

and eliminating ψ_B, we get

$$\begin{pmatrix} R\partial_R + 1 & -l + \frac{g^2(R+1)^2}{l} \\ \frac{R+1}{R} & -\frac{1}{l}[1 + (R+1)\partial_R] \end{pmatrix} \begin{pmatrix} F \\ G \end{pmatrix} = 0. \tag{B5}$$

It is possible to separate G. Especially, from the second equation in Eq. (A8), we get

$$G'' + \left[\frac{1}{R+1} + \frac{2}{R}\right]G' + \left\{\frac{R+2}{R(R+1)^2} - \frac{l^2}{R^2} + g^2\left(1 + \frac{1}{R}\right)^2\right\}G = 0. \tag{B6}$$

Note that the singular behavior is different from that in Eq. (A5) because $R+1$ now becomes a second-order singularity. Using the ansatz

$$\lim_{R\to -1} G \sim (1+R)^x, \tag{B7}$$

we get $x = \pm 1$. However, $x = 1$ is forbidden since the second derivative of the wavefunction at this point is zero, suggesting that the singularity of G occurs at $1/(R+1)$. From Eq. (B5), we have that a similar singularity arises in F, but not in ψ_B.

3. Conductivity and current near $\rho + g = 0$

Equation (B5) indicates the existence of a singularity in ψ_A and ψ_C for $l \neq 0$, which occurs at $\rho + g = 0$. With $\rho = \epsilon r$ and $\epsilon = E/v_F$, we get that the singularity occurs for

$$\frac{E_0}{t} \equiv -\frac{3}{\sqrt{2}}\frac{a}{r}g, \tag{B8}$$

which depends on both the incidence energy E_0 and the measurement point r_0.

The DOS is defined in Eq. (13). For a fixed measurement point r_0, as the energy is changed, ψ_A and ψ_C exhibit a singularity near $E \to E_0$ for $l \neq 0$, which dominates the sum. We thus obtain the behavior of conductivity divergence:

$$\lim_{E\to V(r)} \sigma \sim (E - E_0)^{-2}. \tag{B9}$$

For a fixed energy value, as the measurement position is varied, a singularity will rise in a similar fashion. The current components are defined as

$$\begin{aligned} j_r &= v_F \boldsymbol{\psi}^\dagger \mathbf{S}\cdot\hat{e}_r\boldsymbol{\psi} = \sqrt{2}\mathrm{Re}[\psi_2^*(\psi_1 e^{i\theta} + \psi_3 e^{-i\theta})], \\ j_\theta &= v_F \boldsymbol{\psi}^\dagger \mathbf{S}\cdot\hat{e}_\theta\boldsymbol{\psi} = -\sqrt{2}\mathrm{Im}[\psi_2^*(\psi_1 e^{i\theta} - \psi_3 e^{-i\theta})]. \end{aligned} \tag{B10}$$

Inserting Eq. (4) into the current expressions, we obtain $j_r = 0$ and $j_\theta \sim G$ for real ψ_B (which occurs only in the noncollapse region). Also, from Eq. (B5), we obtain the singularity in G with $G \sim (r - r_0)^{-1}$, indicating a sign change for j_θ near the zero kinetic energy point.

4. The case of $|\rho| \to \infty$

To get the asymptotic behavior, we use the transform

$$w = \frac{R}{\sqrt{R+1}}\psi_B. \tag{B11}$$

Making the change of variable from R to ρ in Eq. (A5), we get

$$w'' + \left(1 + \frac{g}{\rho} + \frac{g^2 - l^2}{\rho^2} + \frac{\frac{1}{4}(\rho + 2g)^2 - g^2}{\rho^2(\rho + g)^2}\right)w = 0. \tag{B12}$$

Because $|\rho| \gg g$, we can approximate Eq. (B12) as

$$w'' + \left(1 + \frac{2\tilde{g}}{|\rho|} + \frac{g^2 - l^2 + 1/4}{\rho^2}\right)w = 0, \tag{B13}$$

where $\tilde{g} = s_\varepsilon g$. Equation (B13) is the Whittaker equation [82], which contains a logarithmic phase shift

$$\psi_B \sim \sqrt{\frac{2}{\pi r}}\cos[|\rho| + \tilde{g}\log(2|\rho|) + \delta_l], \tag{B14}$$

where δ_l is the scattering phase associated with the angular momentum quantum number l.

APPENDIX C: IS THERE DEGENERACY BETWEEN THE $\pm L$ STATES IN PSEUDOSPIN-1/2 AND PSEUDOSPIN-1 SYSTEMS?

The relationship between the l and $-l$ states after collapse depends not only on the angular momentum, but also on the boundary condition. In Refs. [14] and [15], the boundary condition is $\psi_2(a_0) = 0$. This choice leads to the degeneracy of the $l = \pm 1/2$ states in the collapse region.

In our work, we use the zero current boundary condition, as in Refs. [18] and [70]. By setting

$$\psi_2(a_0)/\psi_1(a_0) = i\exp(i\theta),$$

we get a "impenetrable region" around the impurity. This boundary condition was justified by lattice calculation in Ref. [18]. In Ref. [18] and Fig. 19(d) in Ref. [21], it is shown that the density of states is not degenerate under the boundary condition.

We first analyze the degeneracy for pseudospin-1/2 systems with a Coulomb impurity. In such a system, we have

$$v_F(\boldsymbol{\sigma}\cdot\boldsymbol{p} - g/r)\boldsymbol{\Psi}(\boldsymbol{r}) = E\boldsymbol{\Psi}(\boldsymbol{r}), \tag{C1}$$

where $g = Ze^2/\kappa v_F$ and $\epsilon = E/v_F$, as for a pseudospin-1 system. With the two-component spinor wave function

$$\boldsymbol{\Psi}_l(r) = \frac{1}{\sqrt{r}}\begin{pmatrix} e^{i[l-(1/2)]\theta}\psi_l^A(r) \\ ie^{i[l+(1/2)]\theta}\psi_l^B(r) \end{pmatrix}, \tag{C2}$$

the Dirac equation becomes

$$\begin{pmatrix} \epsilon + g/r & -(\partial_r + l/r) \\ (\partial_r - l/r) & \epsilon + g/r \end{pmatrix}\begin{pmatrix} \psi_l^A \\ \psi_l^B \end{pmatrix} = 0. \tag{C3}$$

Under the transform $l \to -l$, we get

$$\begin{aligned} \psi_{-l}^A &= \psi_l^B \\ \psi_{-l}^B &= -\psi_l^A. \end{aligned} \tag{C4}$$

We see that the transform only changes the sign of one component, leading to no difference in the LDOS. For a collapse state, the impenetrable boundary condition implies another equation:

$$\psi_l^A(a_0) = \psi_l^B(a_0). \tag{C5}$$

Comparing this equation with Eq. (C4), we see that the transform $l \to -l$ can no longer maintain the boundary condition. As a result, the degeneracy is broken.

We now turn to the problem of degeneracy in pseudospin-1 systems, where the relation between the Fermi velocity and the hopping energy is $v_F = 3at/\sqrt{2}$. Before collapse, the solution of the wave function is given by Eqs. (6)–(10). Under the transform $l \to -l$, we have

$$\begin{aligned} \psi^A_{-l} &= -\psi^C_l, \\ \psi^B_{-l} &= \psi^B_l, \\ \psi^C_{-l} &= -\psi^A_l. \end{aligned} \tag{C6}$$

As a result, the LDOS is identical for the l and $-l$ states. After collapse, the boundary condition near the impurity is given by

$$2\psi^B_l(a_0) = \psi^A_l(a_0) - \psi^C_l(a_0), \tag{C7}$$

which no longer holds under the transform $l \to -l$. There is then no degeneracy between the l and $-l$ states.

APPENDIX D: RELATIVISTIC QUANTUM TWO-BODY PROBLEM

Following Refs. [69] and [73], we label the wave function for two pseudospin-1/2 particles in graphene with $i, j = (A, B)$. We have

$$\begin{aligned} \Psi_{ij}(\mathbf{r}_1, \mathbf{r}_2) &= \Psi_i(\mathbf{r}_1) \otimes \Psi_j(\mathbf{r}_2) \\ &= (\Psi_{AA}, \Psi_{AB}, \Psi_{BA}, \Psi_{BB})^T. \end{aligned} \tag{D1}$$

Introducing the center-of-mass frame: $\mathbf{R} = (\mathbf{r}_1 + \mathbf{r}_2)/2$ and $\mathbf{r} = \mathbf{r}_1 - \mathbf{r}_2$ with center-of-mass momentum $\hbar\mathbf{K} = 0$, we obtain

$$\begin{pmatrix} \Psi_{AA}(\mathbf{r}_1, \mathbf{r}_2) \\ \Psi_{AB}(\mathbf{r}_1, \mathbf{r}_2) \\ \Psi_{BA}(\mathbf{r}_1, \mathbf{r}_2) \\ \Psi_{BB}(\mathbf{r}_1, \mathbf{r}_2) \end{pmatrix} = \begin{pmatrix} e^{i(l-1)\theta}\phi_1(r) \\ -\frac{i}{2}e^{il\theta}\phi_2(r) \\ \frac{i}{2}e^{il\theta}\phi_2(r) \\ e^{i(l+1)\theta}\phi_3(r) \end{pmatrix}, \tag{D2}$$

where ϕ_1, ϕ_2, ϕ_3 satisfy the equation

$$\begin{pmatrix} \frac{v(r)-E}{\hbar v_F} & \partial_r + \frac{l}{r} & 0 \\ -2\left(\partial_r - \frac{l-1}{r}\right) & \frac{v(r)-E}{\hbar v_F} & 2\left(\partial_r + \frac{l+1}{r}\right) \\ 0 & -\partial_r + \frac{l}{r} & \frac{v(r)-E}{\hbar v_F} \end{pmatrix} \begin{pmatrix} \phi_1(r) \\ \phi_2(r) \\ \phi_3(r) \end{pmatrix} = 0. \tag{D3}$$

Introducing the Coulomb potential $V(r) = Ze^2/\kappa r$ and imposing the normalized units $g_0 = Ze^2/(2\kappa v_F)$ and $\varepsilon_0 = E/(2v_F)$, we see that (ϕ_1, ϕ_2, ϕ_3) correspond to $(\psi_A, 2\psi_B, \psi_C)$.

[1] I. Pomeranchuk and Y. Smorodinsky, On the energy levels of systems with $Z > 137$, J. Phys. USSR **9**, 97 (1945).

[2] Y. B. Zeldovich and V. S. Popov, Electronic structure of superheavy atoms, Sov. Phys. Usp. **14**, 673 (1972).

[3] W. Greiner, B. Muller, and J. Rafelski, *Quantum Electrodynamics of Strong Fields* (Springer-Verlag, Berlin, 1985).

[4] L. D. Landau and E. M. Lifshitz, *Quantum Mechanics: Non-Relativistic Theory* (Pergamon, New York, 1981).

[5] C. G. Darwin, On some orbits of an electron, Philos. Mag. Ser. 6 **25**, 201 (2004).

[6] T. H. Boyer, Unfamiliar trajectories for a relativistic particle in a Kepler or Coulomb potential, Am. J. Phys. **72**, 992 (2004).

[7] K. S. Novoselov, A. K. Geim, S. V. Morozov, D. Jiang, Y. Zhang, S. V. Dubonos, I. V. Grigorieva, and A. A. Firsov, Electric field effect in atomically thin carbon films, Science **306**, 666 (2004).

[8] C. Berger, Z. M. Song, T. B. Li, X. B. Li, A. Y. Ogbazghi, R. F. Z. T. Dai, A. N. Marchenkov, E. H. Conrad, P. N. First, and W. A. de Heer, Ultrathin epitaxial graphite: 2D electron gas properties and a route toward graphene-based nanoelectronics, J. Phys. Chem. B **108**, 19912 (2004).

[9] K. S. Novoselov, A. K. Geim, S. V. Morozov, D. Jiang, M. I. Katsnelson, I. V. Grigorieva, S. V. Dubonos, and A. A. Firsov, Two-dimensional gas of massless Dirac fermions in graphene, Nature **438**, 197 (2005).

[10] Y. B. Zhang, Y. W. Tan, H. L. Stormer, and P. Kim, Experimental observation of the quantum Hall effect and Berry's phase in graphene, Nature **438**, 201 (2005).

[11] A. H. Castro Neto, F. Guinea, N. M. R. Peres, K. S. Novoselov, and A. K. Geim, The electronic properties of graphene, Rev. Mod. Phys. **81**, 109 (2009).

[12] N. M. R. Peres, Colloquium: The transport properties of graphene: An introduction, Rev. Mod. Phys. **82**, 2673 (2010).

[13] S. Das Sarma, S. Adam, E. H. Hwang, and E. Rossi, Electronic transport in two-dimensional graphene, Rev. Mod. Phys. **83**, 407 (2011).

[14] A. V. Shytov, M. I. Katsnelson, and L. S. Levitov, Vacuum Polarization and Screening of Supercritical Impurities in Graphene, Phys. Rev. Lett. **99**, 236801 (2007).

[15] A. V. Shytov, M. I. Katsnelson, and L. S. Levitov, Atomic Collapse and Quasi-Rydberg States in Graphene, Phys. Rev. Lett. **99**, 246802 (2007).

[16] M. M. Fogler, D. S. Novikov, and B. I. Shklovskii, Screening of a hypercritical charge in graphene, Phys. Rev. B **76**, 233402 (2007).

[17] I. S. Terekhov, A. I. Milstein, V. N. Kotov, and O. P. Sushkov, Screening of Coulomb Impurities in Graphene, Phys. Rev. Lett. **100**, 076803 (2008).

[18] V. M. Pereira, J. Nilsson, and A. H. Castro Neto, Coulomb Impurity Problem in Graphene, Phys. Rev. Lett. **99**, 166802 (2007).

[19] A. C. Neto, V. N. Kotov, J. Nilsson, V. M. Pereira, N. M. Peres, and B. Uchoa, Adatoms in graphene, Solid State Commun. **149**, 1094 (2009).

[20] D. S. Novikov, Elastic scattering theory and transport in graphene, Phys. Rev. B **76**, 245435 (2007).

[21] V. N. Kotov, B. Uchoa, V. M. Pereira, F. Guinea, and A. H. Castro Neto, Electron-electron interactions in graphene: Current status and perspectives, Rev. Mod. Phys. **84**, 1067 (2012).

[22] Y. Wang, V. W. Brar, A. V. Shytov, Q. Wu, W. Regan, H.-Z. Tsai, A. Zettl, L. S. Levitov, and M. F. Crommie, Mapping Dirac quasiparticles near a single Coulomb impurity on graphene, Nat. Phys. **8**, 653 (2012).

[23] Y. Wang, D. Wong, A. V. Shytov, V. W. Brar, S. Choi, Q. Wu, H.-Z. Tsai, W. Regan, A. Zettl, R. K. Kawakami *et al.*, Observing atomic collapse resonances in artificial nuclei on graphene, Science **340**, 734 (2013).

[24] J. Mao, Y. Jiang, D. Moldovan, G. Li, K. Watanabe, T. Taniguchi, M. R. Masir, F. M. Peeters, and E. Y. Andrei, Realization of a tunable artificial atom at a supercritically charged vacancy in graphene, Nat. Phys. **12**, 545 (2016).

[25] Y. Jiang, J. Mao, D. Moldovan, M. R. Masir, G. Li, K. Watanabe, T. Taniguchi, F. M. Peeters, and E. Y. Andrei, Tuning a circular p–n junction in graphene from quantum confinement to optical guiding, Nat. Nanotechnol. **12**, 1045 (2017).

[26] O. Ovdat, J. Mao, Y. Jiang, E. Andrei, and E. Akkermans, Observing a scale anomaly and a universal quantum phase transition in graphene, Nat. Commun. **8**, 507 (2017).

[27] D. Bercioux, D. F. Urban, H. Grabert, and W. Häusler, Massless Dirac-Weyl fermions in a T_3 optical lattice, Phys. Rev. A **80**, 063603 (2009).

[28] R. Shen, L. B. Shao, B. Wang, and D. Y. Xing, Single Dirac cone with a flat band touching on line-centered-square optical lattices, Phys. Rev. B **81**, 041410(R) (2010).

[29] D. Green, L. Santos, and C. Chamon, Isolated flat bands and spin-1 conical bands in two-dimensional lattices, Phys. Rev. B **82**, 075104 (2010).

[30] B. Dóra, J. Kailasvuori, and R. Moessner, Lattice generalization of the Dirac equation to general spin and the role of the flat band, Phys. Rev. B **84**, 195422 (2011).

[31] F. Wang and Y. Ran, Nearly flat band with Chern number $c = 2$ on the dice lattice, Phys. Rev. B **84**, 241103(R) (2011).

[32] X. Huang, Y. Lai, Z. H. Hang, H. Zheng, and C. T. Chan, Dirac cones induced by accidental degeneracy in photonic crystals and zero-refractive-index materials, Nat. Mater. **10**, 582 (2011).

[33] J. Mei, Y. Wu, C. T. Chan, and Z.-Q. Zhang, First-principles study of Dirac and Dirac-like cones in phononic and photonic crystals, Phys. Rev. B **86**, 035141 (2012).

[34] P. Moitra, Y. Yang, Z. Anderson, I. I. Kravchenko, D. P. Briggs, and J. Valentine, Realization of an all-dielectric zero-index optical metamaterial, Nat. Photon. **7**, 791 (2013).

[35] M. Vigh, L. Oroszlány, S. Vajna, P. San-Jose, G. Dávid, J. Cserti, and B. Dóra, Diverging dc conductivity due to a flat band in a disordered system of pseudospin-1 dirac-weyl fermions, Phys. Rev. B **88**, 161413(R) (2013).

[36] D. Guzmán-Silva, C. Mejía-Cortés, M. A. Bandres, M. C. Rechtsman, S. Weimann, S. Nolte, M. Segev, A. Szameit, and R. A. Vicencio, Experimental observation of bulk and edge transport in photonic Lieb lattices, New J. Phys. **16**, 063061 (2014).

[37] J. Romhányi, K. Penc, and R. Ganesh, Hall effect of triplons in a dimerized quantum magnet, Nat. Commun. **6**, 6805 (2015).

[38] G. Giovannetti, M. Capone, J. van den Brink, and C. Ortix, Kekulé textures, pseudospin-one Dirac cones, and quadratic band crossings in a graphene-hexagonal indium chalcogenide bilayer, Phys. Rev. B **91**, 121417(R) (2015).

[39] Y. Li, S. Kita, P. Muoz, O. Reshef, D. I. Vulis, M. Yin, M. Lonar, and E. Mazur, On-chip zero-index metamaterials, Nat. Photon. **9**, 738 (2015).

[40] S. Mukherjee, A. Spracklen, D. Choudhury, N. Goldman, P. Öhberg, E. Andersson, and R. R. Thomson, Observation of a Localized Flat-Band State in a Photonic Lieb Lattice, Phys. Rev. Lett. **114**, 245504 (2015).

[41] R. A. Vicencio, C. Cantillano, L. Morales-Inostroza, B. Real, C. Mejía-Cortés, S. Weimann, A. Szameit, and M. I. Molina, Observation of Localized States in Lieb Photonic Lattices, Phys. Rev. Lett. **114**, 245503 (2015).

[42] S. Taie, H. Ozawa, T. Ichinose, T. Nishio, S. Nakajima, and Y. Takahashi, Coherent driving and freezing of bosonic matter wave in an optical Lieb lattice, Sci. Adv. **1**, e1500854 (2015).

[43] W. Häusler, Flat-band conductivity properties at long-range Coulomb interactions, Phys. Rev. B **91**, 041102(R) (2015).

[44] A. Fang, Z. Q. Zhang, S. G. Louie, and C. T. Chan, Klein tunneling and supercollimation of pseudospin-1 electromagnetic waves, Phys. Rev. B **93**, 035422 (2016).

[45] F. Diebel, D. Leykam, S. Kroesen, C. Denz, and A. S. Desyatnikov, Conical Diffraction and Composite Lieb Bosons in Photonic Lattices, Phys. Rev. Lett. **116**, 183902(R) (2016).

[46] L. Zhu, S.-S. Wang, S. Guan, Y. Liu, T. Zhang, G. Chen, and S. A. Yang, Blue phosphorene oxide: Strain-tunable quantum phase transitions and novel 2D emergent fermions, Nano Lett. **16**, 6548 (2016).

[47] B. Bradlyn, J. Cano, Z. Wang, M. G. Vergniory, C. Felser, R. J. Cava, and B. A. Bernevig, Beyond Dirac and Weyl fermions: Unconventional quasiparticles in conventional crystals, Science **353**, aaf5037 (2016).

[48] H.-Y. Xu and Y.-C. Lai, Revival resonant scattering, perfect caustics, and isotropic transport of pseudospin-1 particles, Phys. Rev. B **94**, 165405 (2016).

[49] I. C. Fulga and A. Stern, Triple point fermions in a minimal symmorphic model, Phys. Rev. B **95**, 241116(R) (2017).

[50] M. Ezawa, Triplet fermions and Dirac fermions in borophene, Phys. Rev. B **96**, 035425 (2017).

[51] C. Zhong, Y. Chen, Z.-M. Yu, Y. Xie, H. Wang, S. A. Yang, and S. Zhang, Three-dimensional pentagon carbon with a genesis of emergent fermions, Nat. Commun. **8**, 15641 (2017).

[52] Y.-Q. Zhu, D.-W. Zhang, H. Yan, D.-Y. Xing, and S.-L. Zhu, Emergent pseudospin-1 Maxwell fermions with a threefold degeneracy in optical lattices, Phys. Rev. A **96**, 033634 (2017).

[53] R. Drost, T. Ojanen, A. Harju, and P. Liljeroth, Topological states in engineered atomic lattices, Nat. Phys. **13**, 668 (2017).

[54] M. R. Slot, T. S. Gardenier, P. H. Jacobse, G. C. P. van Miert, S. N. Kempkes, S. J. M. Zevenhuizen, C. M. Smith, D. Vanmaekelbergh, and I. Swart, Experimental realization and characterization of an electronic Lieb lattice, Nat. Phys. **13**, 672 (2017).

[55] H.-Y. Xu and Y.-C. Lai, Superscattering of a pseudospin-1 wave in a photonic lattice, Phys. Rev. A **95**, 012119 (2017).

[56] C.-Z. Wang, H.-Y. Xu, L. Huang, and Y.-C. Lai, Nonequilibrium transport in the pseudospin-1 Dirac-Weyl system, Phys. Rev. B **96**, 115440 (2017).

[57] X. Tan, D.-W. Zhang, Q. Liu, G. Xue, H.-F. Yu, Y.-Q. Zhu, H. Yan, S.-L. Zhu, and Y. Yu, Topological Maxwell Metal Bands in a Superconducting Qutrit, Phys. Rev. Lett. **120**, 130503 (2018).

[58] B. Sutherland, Localization of electronic wave functions due to local topology, Phys. Rev. B **34**, 5208 (1986).
[59] E. Illes and E. J. Nicol, Magnetic properties of the $\alpha - T_3$ model: Magneto-optical conductivity and the Hofstadter butterfly, Phys. Rev. B **94**, 125435 (2016).
[60] J. D. Malcolm and E. J. Nicol, Frequency-dependent polarizability, plasmons, and screening in the two-dimensional pseudospin-1 dice lattice, Phys. Rev. B **93**, 165433 (2016).
[61] A. A. Burkov and E. Demler, Vortex-Peierls States in Optical Lattices, Phys. Rev. Lett. **96**, 180406 (2006).
[62] A. Raoux, M. Morigi, J.-N. Fuchs, F. Piéchon, and G. Montambaux, From Dia-To Paramagnetic Orbital Susceptibility of Massless Fermions, Phys. Rev. Lett. **112**, 026402 (2014).
[63] D. Leykam and S. Flach, Perspective: Photonic flatbands, APL Photon. **3**, 070901 (2018).
[64] S. Mukherjee, M. Di Liberto, P. Öhberg, R. R. Thomson, and N. Goldman, Experimental Observation of Aharonov-Bohm Cages in Photonic Lattices, Phys. Rev. Lett. **121**, 075502 (2018).
[65] A. Ronveaux and F. M. Arscott, *Heuns Differential Equations* (Oxford University Press, Oxford, UK, 1995).
[66] S.-H. Dong, *Factorization Method in Quantum Mechanics*, Vol. 150 (Springer Science & Business Media, New York, 2007).
[67] E. S. Cheb-Terrab, Solutions for the general, confluent and biconfluent Heun equations and their connection with Abel equations, J. Phys. A **37**, 9923 (2004).
[68] P. P. Fiziev, Novel relations and new properties of confluent Heun's functions and their derivatives of arbitrary order, J. Phys. A: Math. Theor. **43**, 035203 (2009).
[69] J. Sabio, F. Sols, and F. Guinea, Two-body problem in graphene, Phys. Rev. B **81**, 045428 (2010).
[70] J. Wang, H. A. Fertig, and G. Murthy, Critical Behavior in Graphene with Coulomb Interactions, Phys. Rev. Lett. **104**, 186401 (2010).
[71] M. V. Berry and R. Mondragon, Neutrino billiards: Time-reversal symmetry-breaking without magnetic fields, Proc. R. Soc. London A **412**, 53 (1987).
[72] M. Ouyang, J.-L. Huang, and C. M. Lieber, One-Dimensional Energy Dispersion of Single-Walled Carbon Nanotubes by Resonant Electron Scattering, Phys. Rev. Lett. **88**, 066804 (2002).
[73] C. Downing and M. Portnoi, Bielectron vortices in two-dimensional Dirac semimetals, Nat. Commun. **8**, 897 (2017).
[74] C. A. Downing, Two-electron atom with a screened interaction, Phys. Rev. A **95**, 022105 (2017).
[75] A. De Martino and R. Egger, Two-electron bound states near a Coulomb impurity in gapped graphene, Phys. Rev. B **95**, 085418 (2017).
[76] H. A. Olsen, P. Osland, and T. T. Wu, On the existence of bound states for a massive spin-one particle and a magnetic monopole, Phys. Rev. D **42**, 665 (1990).
[77] H. A. Olsen and P. Osland, Bound states for a massive spin-one particle and a magnetic monopole, Phys. Rev. D **42**, 690 (1990).
[78] M. L. Horner and A. S. Goldhaber, Aharonov-Bohm problem for spin 1, Phys. Rev. D **55**, 5951 (1997).
[79] I. Boztosun, M. Karakoc, F. Yasuk, and A. Durmus, Asymptotic iteration method solutions to the relativistic Duffin-Kemmer-Petiau equation, J. Math. Phys. **47**, 062301 (2006).
[80] H. Hassanabadi, B. H. Yazarloo, S. Zarrinkamar, and A. A. Rajabi, Duffin-Kemmer-Petiau equation under a scalar Coulomb interaction, Phys. Rev. C **84**, 064003 (2011).
[81] R. Van Pottelberge, M. Zarenia, P. Vasilopoulos, and F. M. Peeters, Graphene quantum dot with a Coulomb impurity: Subcritical and supercritical regime, Phys. Rev. B **95**, 245410 (2017).
[82] F. W. Olver, D. W. Lozier, R. F. Boisvert, and C. W. Clark, *NIST Handbook of Mathematical Functions* (Cambridge University Press, New York, 2010).